

## Article

# Hydrothermal Synthesis of Cancrinite from Coal Gangue for the Immobilization of Sr

Hao Wang, Fujie Zhang, Ran Ang and Ding Ren \*

Key Laboratory of Radiation Physics and Technology of Ministry of Education, Institute of Nuclear Science and Technology, Sichuan University, Chengdu 610065, China; wanghao720@stu.scu.edu.cn (H.W.); zhangfujie131@163.com (F.Z.); rang@scu.edu.cn (R.A.)

\* Correspondence: rending2k@scu.edu.cn

**Abstract:** The primary objective of this study is to investigate and develop a rapid and effective method for the immobilization of Sr in the event of a nuclear leakage incident. Coal gangue, an underutilized form of solid waste from the coal industry, can be used as a raw material for curing Sr due to its high content of silica–alumina oxides. In the present study, Sr was successfully solidified in cancrinite synthesized using a hydrothermal method with coal gangue as raw material. A stable cancrinite phase was formed at a relative alkali concentration of more than 6 M. When the Sr/Al(Si) ratio was <1/6, cancrinite was the only stable phase that varied with the hydrothermal temperature and time. When the Sr/Al(Si) ratio increased to 1/2, the cancrinite phase completely disappeared, and a new strontium feldspar phase ( $\text{SrAl}_2\text{Si}_2\text{O}_8$ ) appeared. PCT leaching experiments showed that when  $\text{Sr/Al(Si)} < 1/6$ , the Sr leaching rate of Sr-cancrinite samples obtained by hydrothermal synthesis at 180 °C for 24 h was very low.

**Keywords:** coal gangue; cancrinite; hydrothermal synthesis; Sr; emergency curing

## 1. Introduction



**Citation:** Wang, H.; Zhang, F.; Ang, R.; Ren, D. Hydrothermal Synthesis of Cancrinite from Coal Gangue for the Immobilization of Sr. *Materials* **2024**, *17*, 573. <https://doi.org/10.3390/ma17030573>

Academic Editor: Francesco Caridi

Received: 6 December 2023

Revised: 20 January 2024

Accepted: 23 January 2024

Published: 25 January 2024



**Copyright:** © 2024 by the authors. Licensee MDPI, Basel, Switzerland. This article is an open access article distributed under the terms and conditions of the Creative Commons Attribution (CC BY) license (<https://creativecommons.org/licenses/by/4.0/>).

Nuclear energy represents a highly concentrated and versatile energy source with extensive potential for application [1]. However, the development and utilization of nuclear technology, while yielding economic and societal benefits, also entail the inherent risk of nuclear accidents [2,3]. One such hazard involves the presence of  $^{90}\text{Sr}$ , a prominent constituent found in spent nuclear fuel, high-level liquid waste (HLLW) resulting from spent nuclear fuel reprocessing, and other waste materials generated during reactor operation [4,5]. In waste,  $^{90}\text{Sr}$  typically exists in ionic form and demonstrates strong migration capabilities in water [6]. In the event of a nuclear accident, the decay heat of radioactive strontium accelerates its diffusion and migration, posing severe consequences if the nuclide enters the biosphere [7]. During an emergency nuclear spill, the HLLW typically exhibits high mobility, making it challenging to collect and isolate effectively [8]. Consequently, a recommended approach involves the expedient solidification of the radionuclides present in the HLLW, evaluating their concentrations, and thereby diminishing its potential hazards for subsequent disposal purposes [9]. It is imperative for the development of nuclear energy to conduct applied basic research on the emergency treatment of radioactive strontium in leaking waste from nuclear accidents, as well as to develop rapid and efficient materials for nuclear emergency treatment.

The utilization of Synroc solidification techniques for certain radionuclides has demonstrated remarkable performance and holds significant prospects for further advancement [10–15]. The essence of its solidification treatment is to form a certain solid solution of the radionuclides in high-level liquid waste with the corresponding salts in the high-temperature phase, thereby encapsulating the radionuclides in the solid phase and creating a thermodynamically stable solidified matrix [16–19]. Researchers have employed natural zeolite as an adsorption material to effectively remove  $\text{Sr}^{2+}$  and  $\text{Cs}^+$  ions from aqueous

solutions, yielding positive outcomes [20]. Cancrinite, an exceptional zeolite, exhibits an open framework structure comprising hexagonal rings of  $\text{SiO}_4$  and  $\text{AlO}_4$  tetrahedra stacked along the hexagonal c-axis [21–23]. This structure forms small  $\varepsilon$ -cages and a large 12-ring channel along the c-axis [24,25]. The incorporation of  $\text{Sr}^{2+}$  ions into this structural framework is feasible [26–29]. The synthesis of cancrinite is relatively straightforward, employing hydrothermal or high-temperature calcination methods with diverse raw materials, such as silicon and aluminum sources dissolved in  $\text{NaOH}$  solution, along with specific anions [30–33]. Coal gangue (CG), a solid waste generated during coal mining, represents a promising resource for utilization [34–36]. However, scarce reports exist on utilizing CG as a raw material for solidifying radioactive waste. Notably, the Sr/Al molar ratio in CG is approximately 1, which closely aligns with the Sr/Al molar ratio observed in cancrinite [37,38]. Therefore, CG holds potential as a viable raw material for the synthesis of cancrinite for the purpose of solidifying Sr radionuclides.

This paper reports on the successful preparation of cancrinite for the solidification of  $\text{Sr}^{2+}$  from Sr nitrate using hydrothermal treatment of CG. The study also investigates the effects of alkali activator concentration, crystallization temperature, and time on cancrinite synthesis, and assesses the maximum Sr capacity and chemical durability of cancrinite synthesized from CG using the PCT method.

## 2. Materials and Methods

### 2.1. Raw Material

The CG samples used in this study were obtained from Shanxi Province. Their chemical and mineral compositions were determined through powder X-ray fluorescence (XRF) and X-ray diffraction (XRD), respectively. The results are presented in Table 1 and Figure 1.

**Table 1.** The main chemical composition of coal gangue (wt%).

Ingredients	$\text{SiO}_2$	$\text{Al}_2\text{O}_3$	$\text{TiO}_2$	$\text{Fe}_2\text{O}_3$	$\text{K}_2\text{O}$	$\text{CaO}$	$\text{MgO}$	$\text{Na}_2\text{O}$	C
Natural CG	42.93	30.20	0.88	0.58	0.43	0.36	0.15	0.10	5.29
Calcined CG	47.15	34.58	1.01	0.73	0.45	0.42	0.17	0.10	1.31

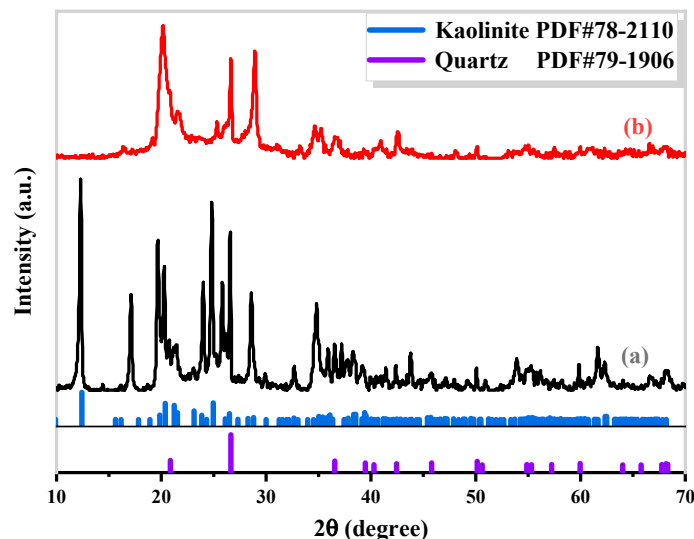


**Figure 1.** XRD spectra of the coal gangue (a) and coal gangue calcined at 900 °C for 5 h (b).

The main chemical components of CG were found to be  $\text{SiO}_2$  (42.93 wt%) and  $\text{Al}_2\text{O}_3$  (30.20 wt%), as expected. After 5 h of decarburization calcination at 900 °C, the contents of  $\text{SiO}_2$  and  $\text{Al}_2\text{O}_3$  in CG increased to 47.15 wt% and 34.58 wt%, respectively. The resulting Al/Si molar ratio was approximately 1, and no additional Si and Al sources were required.

XRD analysis of CG before and after calcination (Figure 1) revealed that the dominant minerals in natural CG were kaolinite and quartz. The calcined sample displayed the characteristics of an X-ray amorphous state, except for some platelet diffraction peaks of quartz, with no obvious crystal diffraction peaks. This indicates that the calcination treatment destroyed the initially stable crystal structure of CG, enhancing its activity and contributing to the formation of silicate and aluminate monomers through fusion with alkali. To enhance the purity of cancrinite crystals, calcined CG was employed as the raw material in this experiment.

## 2.2. Experimental Section

### 2.2.1. Hydrothermal Processing

Calcined CG was combined with  $\text{Sr}(\text{NO}_3)_2$  at specific Sr/Al(Si) molar ratios to serve as the initial materials. This blend was subsequently mixed with NaOH at a predetermined molar ratio. The resulting mixture underwent thorough stirring, facilitated by a magnetic agitator, after the addition of the appropriate quantity of deionized water to achieve uniform pastes. These pastes were molded into cubes ( $1 \times 1 \times 1 \text{ cm}$ ) and left undisturbed at room temperature overnight. Upon demolding, the specimen underwent curing in a Teflon-lined hydrothermal reactor exposed to saturated steam pressure ranging from room temperature to  $180^\circ\text{C}$  for a duration spanning 0 to 24 h. Post-hydrothermal treatment, the synthesized samples were dried at  $105^\circ\text{C}$  for 8 h to facilitate subsequent measurement and characterization.

The detailed process used for the hydrothermal synthesis of Sr-cancrinite is illustrated in Figure 2.

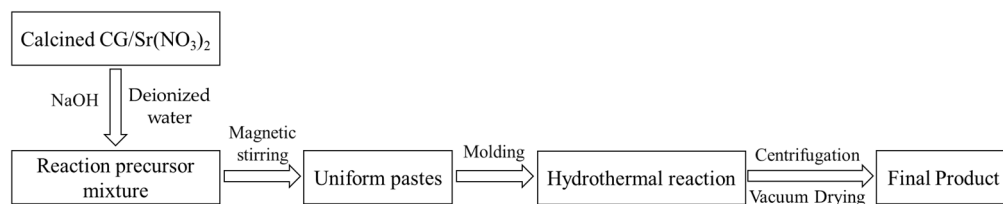


**Figure 2.** Sr-cancrinite hydrothermal synthesis process flowchart.

### 2.2.2. Single Factor Test

The study systematically explored the effects of NaOH concentration, crystallization temperature, and crystallization time on the immobilization of  $\text{Sr}^{2+}$ . Initially, to assess the influence of NaOH concentration on cancrinite's crystallinity and purity, experiments were conducted at  $180^\circ\text{C}$  for 24 h with varying relative molar concentrations from 0 to 8 M of NaOH. Subsequently, the impact of the crystallization temperature was examined by varying the temperature from 90 to  $180^\circ\text{C}$  under a fixed 6 M NaOH concentration for 24 h. Following this, the influence of crystallization time on cancrinite synthesis was investigated by setting the time from 0 to 24 h under 6 M NaOH at  $180^\circ\text{C}$ . Finally, the study delved into the effects of Sr/Al(Si) ratios on cancrinite formation, systematically varying the ratios as 0, 1/6, 1/3, 1/2, and 2/3. This comprehensive series of experiments was designed to pinpoint the optimal conditions for the effective immobilization of  $\text{Sr}^{2+}$ .

### 2.2.3. Sample Characterization and Chemical Durability Testing

The samples underwent characterization of their crystalline phases and morphology using X-ray diffractometry (XRD, EMPYREAN, PANalytical, Almelo, The Netherlands) for phase identification and scanning electron microscopy (SEM, JEOL, JSM-T001F, Tokyo, Japan) for morphology analysis. The chemical stability of Sr-cancrinite was evaluated using the product consistency test (PCT) leaching method [39].

Ion leaching tests were conducted by grinding and filtering the samples through a 100–200 mesh sifter. Subsequently, 1 g of the resulting powder was mixed with 10 mL of deionized water in a Teflon container. The sealed Teflon container was then placed into

a stainless vessel and maintained at 363 K for a duration of  $168 \pm 1$  h. The concentration of  $\text{Sr}^{2+}$  in the leaching solution was analyzed via inductively coupled plasma emission spectrometry (ICP-OES, Agilent 720, Santa Clara, CA, USA). Normalization of the sample concentrations was performed using Equation (1):

$$NC_i = \frac{C_i}{f_i} \quad (1)$$

where  $NC_i$  is the normalized concentration of element  $i$  in the leachate ( $\text{g}\cdot\text{L}^{-1}$ ),  $C_i$  is the concentration of element  $i$  in the leachate ( $\text{g}\cdot\text{L}^{-1}$ ), and  $f_i$  is the mass fraction of element  $i$  in the sample.

### 3. Results and Discussion

#### 3.1. The Effect of NaOH

The synthesis of Sr-cancrinite is greatly influenced by the concentration of NaOH due to the framework structure of cancrinite. In order to investigate this effect, the NaOH concentration was varied between 0–8 M while keeping all other conditions constant. Figure 3 presents the XRD patterns of the samples obtained at different NaOH concentrations, while Figure 4 displays the corresponding SEM images.

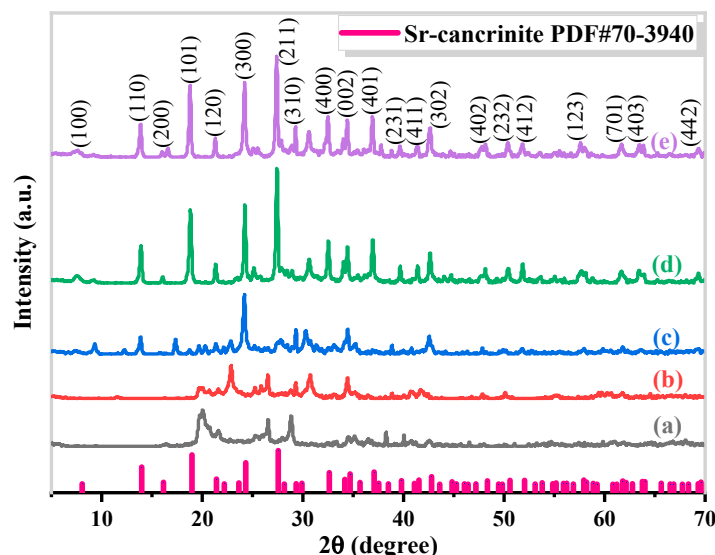


**Figure 3.** XRD patterns of specimens obtained under different NaOH concentrations when the crystallization temperature and crystallization time were 180 °C and 24 h, respectively (NaOH concentrations: (a) 0 M, (b) 2 M, (c) 4 M, (d) 6 M, and (e) 8 M).

The XRD patterns in Figure 3a show that the samples existed in an amorphous form similar to the calcined CG before NaOH was added. The SEM images in Figure 4a,b indicate the absence of regular crystals when the NaOH concentration was less than 4 M, and Figure 4c shows only a small amount of columnar cancrinite crystals. However, at a NaOH concentration of 6 M, diffraction peaks of cancrinite crystals were observed, as shown in Figure 3d and reflected in Figure 4d. When the NaOH concentration was 4 M, the grains were less developed, but the number of smooth columnar crystals increased when the NaOH concentration was increased to above 6 M. This observation indicates that cancrinite can be easily synthesized from CG when a sufficient alkali activator is used. The alkali activator induces the dissolution of silica–alumina oxides in CG and enables sufficient synthesis of silica and aluminum tetrahedra to form the silica–alumina cage structure of cancrinite. Furthermore, the ideal chemical formula of Sr-cancrinite [ $\text{Na}_6\text{Sr}(\text{AlSiO}_4)_6(\text{NO}_3)_2$ ] indicates coordination numbers of eight for cations and two for anions. In order to satisfy the chemical stability of the Al-Si framework, six cations supplied by NaOH are required

to occupy the remaining cation sites, in addition to Sr ions occupying two ionic bonding positions. The synthesized Sr-cancrinite crystals were observed to have a higher particle count and purity when the NaOH concentration was 6 M. Therefore, this concentration was chosen to ensure the reproducibility and consistency of subsequent experiments.

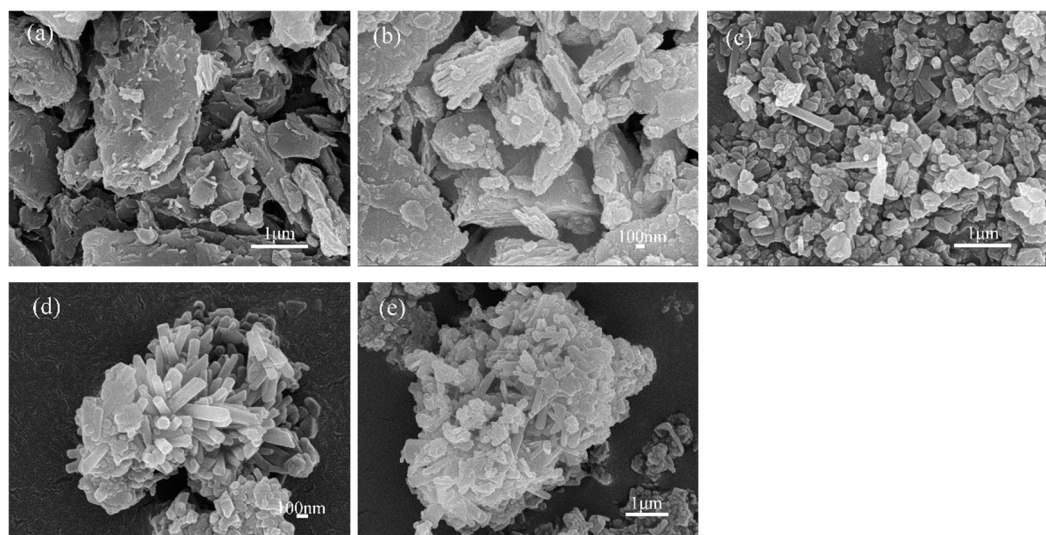


**Figure 4.** SEM photos of specimens obtained under different NaOH concentrations when the crystallization temperature and crystallization time were 180 °C and 24 h, respectively (NaOH concentrations: (a) 0 M, (b) 2 M, (c) 4 M, (d) 6 M, and (e) 8 M).

### 3.2. The Effect of Hydrothermal Temperature and Time

The formation process of Sr-cancrinite grains is primarily determined by the rate of aluminosilicate gel formation and nucleus growth during hydrothermal treatment, and increasing the hydrothermal temperature can accelerate the synthesis process [40]. Moreover, as hydrothermal time and temperature change, the crystals may undergo phase transformation. To investigate the effects of both the crystallization temperature and time on the synthesis of Sr-cancrinite, the crystallization temperature was raised from room temperature to 180 °C, and the crystallization time was increased from 0 to 24 h while keeping other conditions constant. Figures 5 and 6 display the XRD results and SEM photographs of the Sr-cancrinite samples prepared at different temperatures.

The XRD patterns reveal that the crystalline phase before hydrothermal treatment is primarily Sr-cancrinite with small amounts of quartz and sodium nitrate. The diffraction peaks of quartz and sodium nitrate vanished when the hydrothermal temperature was increased to 120 °C. Moreover, the intensity of the diffraction peaks of Sr-cancrinite increased with the rise in the hydrothermal temperature. By analyzing XRD images, the average grain sizes of cancrinite prepared at room temperature and 180 °C were estimated to be around 384 Å and 460 Å, respectively, indicating that increasing the temperature promoted the growth of grains. Furthermore, SEM images showed that numerous small, spherical crystals existed at room temperature, which gradually grew into short rod-shaped crystals with the increase in temperature and ultimately developed into hexagonal long columnar crystals with characteristic morphology.

Figures 7 and 8 present the XRD patterns and SEM images, respectively, of Sr-cancrinite samples prepared at various hydrothermal times.

Before hydrothermal treatment (0 h), the XRD patterns showed the presence of a Sr-cancrinite phase, along with a small amount of quartz and sodium nitrate. After 3 h of hydrothermal treatment, the quartz and sodium nitrate phases disappeared. Additionally, the peak intensity of Sr-cancrinite increased progressively with the increasing curing time. The SEM images depicted the formation of small, spherical grains in the sample without hydrothermal treatment, which subsequently evolved into short, rod-shaped grains with

time. Finally, after 24 h of hydrothermal treatment, the grain morphology transformed into smooth, long columnar crystals.

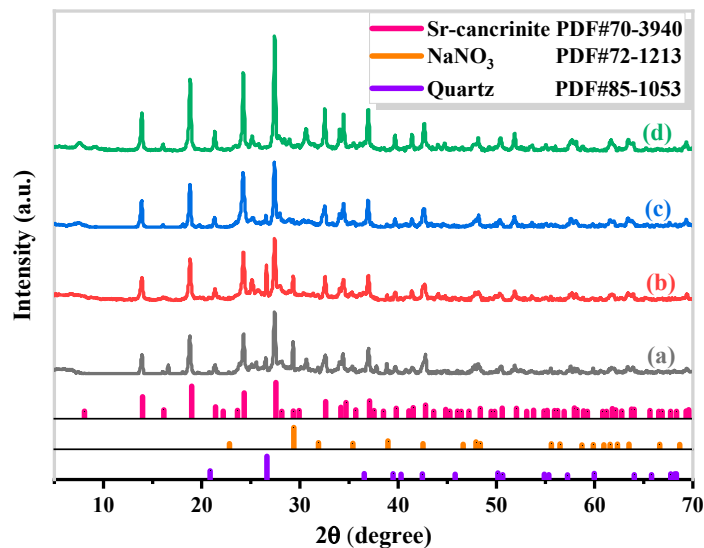


**Figure 5.** XRD patterns of specimens obtained under different crystallization temperatures when NaOH concentration and crystallization time were 6 M and 24 h, respectively (crystallization temperatures: (a) 30 °C, (b) 90 °C, (c) 120 °C, and (d) 180 °C).

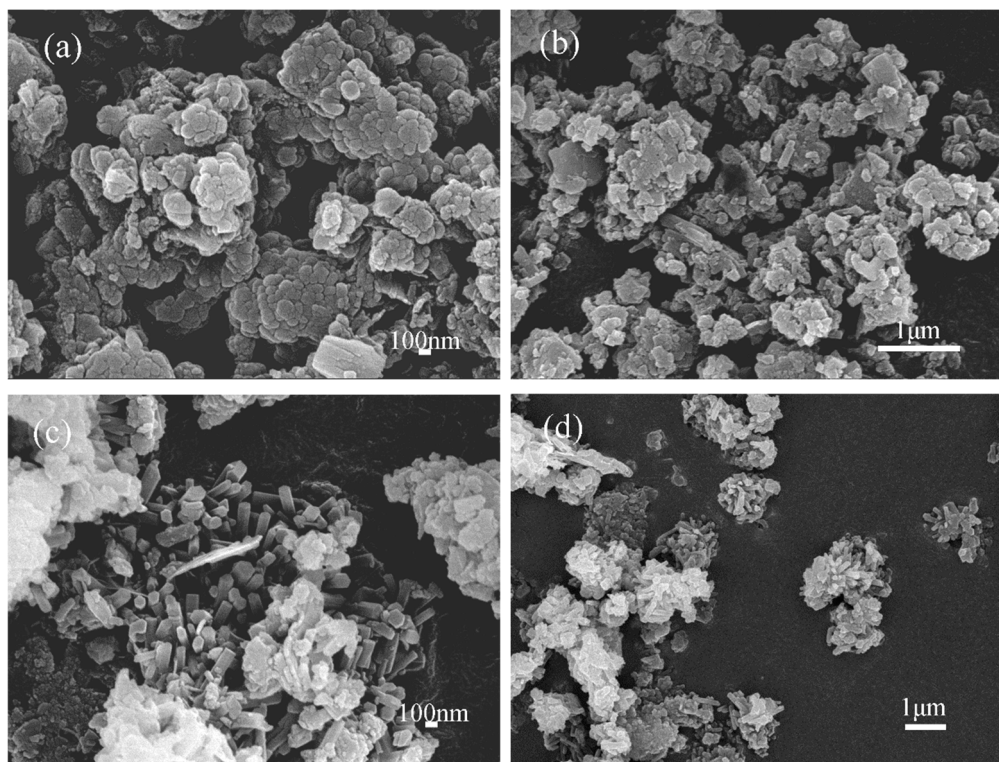


**Figure 6.** SEM photos of specimens obtained under different crystallization temperatures when NaOH concentration and crystallization time were 6 M and 24 h, respectively (crystallization temperatures: (a) 30 °C, (b) 90 °C, (c) 120 °C, and (d) 180 °C).

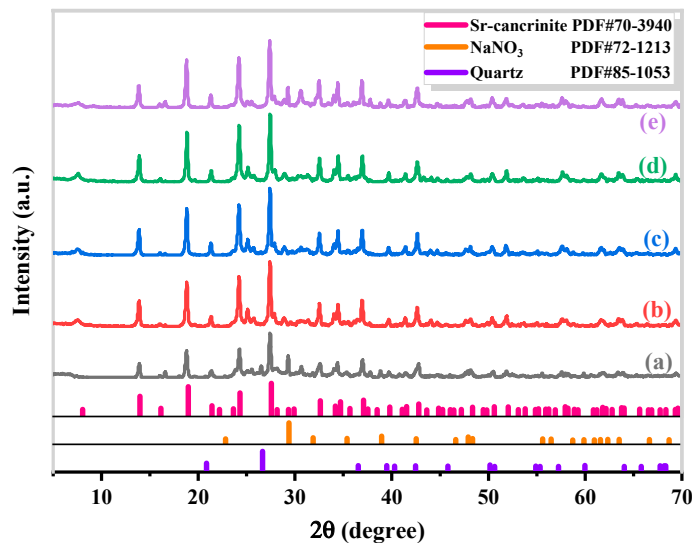


**Figure 7.** XRD patterns of specimens obtained under different crystallization times when NaOH concentration and crystallization temperature were 6 M and 180 °C, respectively (crystallization times: (a) 0 h, (b) 3 h, (c) 6 h, (d) 12 h, and (e) 24 h).

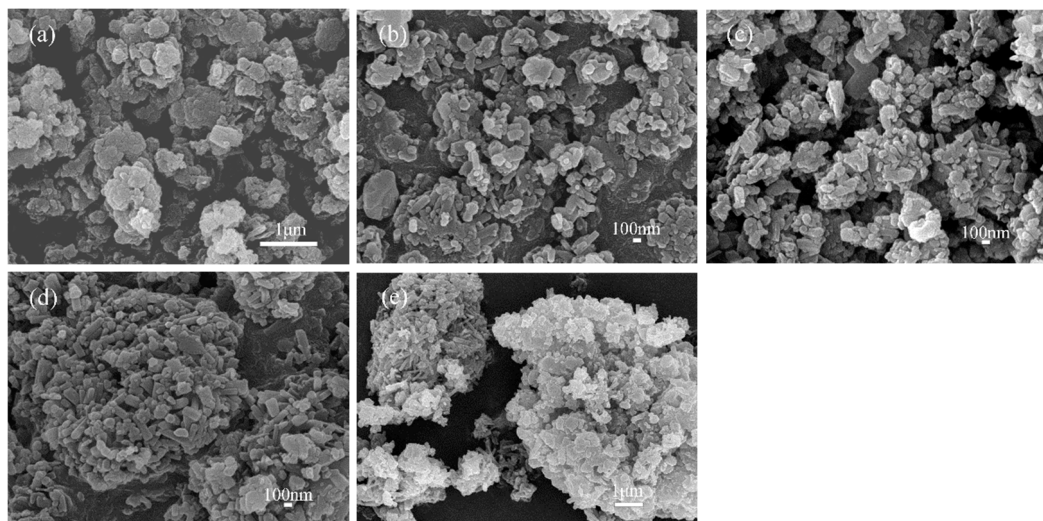


**Figure 8.** SEM photos of specimens obtained under different crystallization times when NaOH concentration and crystallization temperature were 6 M and 180 °C, respectively (crystallization times: (a) 0 h, (b) 3 h, (c) 6 h, (d) 12 h, and (e) 24 h).

The results of the experimental study indicate that the formation of stable Sr-cancrinite is strongly influenced by the curing temperature and time. Based on these results, the optimal conditions for crystallization were determined to be 180 °C and 24 h. Previous research on hydrothermal treatment with different silica–alumina sources for solidifying inorganic waste materials has shown that an acicular zeolite phase transforms to the sodalite phase, eventually leading to the formation of a stable cancrinite phase as the temperature and time are increased [41]. However, in the current study, stable Sr-cancrinite was already present before hydrothermal treatment, and no transformation of the relevant phases was observed. This can be attributed to two factors. Firstly, the Si/Al molar ratio of the starting material was around 1, similar to the structure of cancrinite. Consequently, stable cancrinite crystal nuclei formed at the initial stage of the reaction, followed by hydrothermal time and temperature, which only promoted the ordered growth of the crystals without leading to further phase transformation. During this process, Sr<sup>2+</sup> ions entered the lattice structure of cancrinite from the open interlayer domains of zeolite and occupied the lattice cage. The

localization and fixation of  $\text{Sr}^{2+}$  were achieved through various polar interactions, including ion–ion interactions, electric dipole–electric dipole interactions, and electric dipole–ion interactions. Secondly, the cancrinite phase was thermodynamically stable, and even under hydrothermal conditions, the energy generated by temperature and pressure could not overcome the phase transition potential of cancrinite or lead to its transformation into other phases.

### 3.3. Effect of Sr/Al(Si) Molar Ratio

Based on the molecular composition of cancrinite, it can theoretically incorporate four divalent Sr ions into its silica–aluminum framework. To determine the maximum Sr content that can be accommodated, samples were prepared by controlling the Sr/Al(Si) molar ratio in the range of 0–2/3, followed by curing at 180 °C for 24 h. The phase evolution of the samples was investigated using XRD analysis (Figure 9), revealing that a pure and stable Sr-cancrinite phase existed when the Sr/Al(Si) molar ratio was less than 1/6.

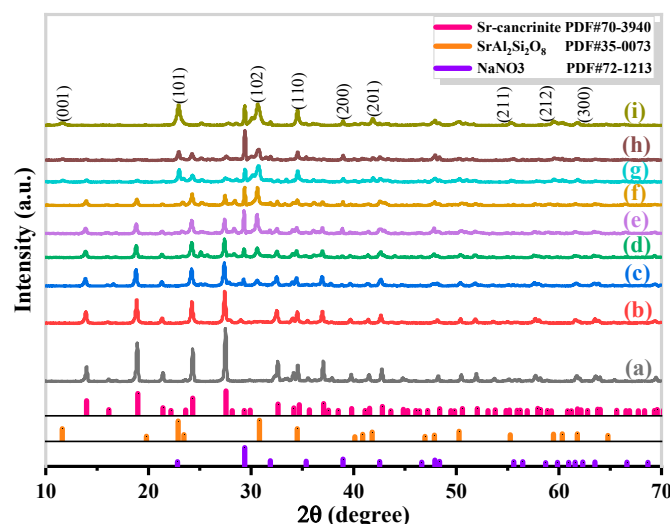


**Figure 9.** XRD patterns of specimens obtained under different Sr/Al(Si) ratios when NaOH concentration, crystallization temperature, and crystallization time were 6 M, 180 °C, and 24 h, respectively (Sr/Al(Si) ratios: (a) 0, (b) 1/12, (c) 1/6, (d) 1/4, (e) 1/3, (f) 5/12, (g) 1/2, (h) 7/12, and (i) 2/3).

However, as the Sr/Al(Si) molar ratio increased, the diffraction peak intensity of the sodium nitrate phase increased, and a new strontium feldspar phase ( $\text{SrAl}_2\text{Si}_2\text{O}_8$ ) appeared when the ratio reached 1/2. SEM images (Figure 10) confirmed these findings, showing smooth, long columnar cancrinite crystals when Sr/Al(Si) was 1/6 and 1/3, but no representative strontium feldspar crystal structure was observed.

The Sr content in the samples was quantified using ICP analysis (Figure 11), which showed that the maximum cured molar fraction of  $\text{Sr}^{2+}$  was about 1/3 of Al(Si), and the ratio of  $\text{Sr}^{2+}$  doping to a cured amount decreased significantly when Sr/Al(Si) was greater than 1/6.

The adsorption of  $\text{Sr}^{2+}$  into the cancrinite crystal structure formed bonds with Al or Si in the lattice, and the bonding strength between Sr and Al or Si was affected by the concentration of  $\text{Sr}^{2+}$  and the coordination number between  $\text{Sr}^{2+}$  and Al or Si. Thus, the amount of  $\text{Sr}^{2+}$  addition and the coordination mode can significantly affect the stability of the cancrinite structure and the interaction of the crystal structure during the curing process.

The experimental results indicate that the quantity of radioactive cations present in cancrinite is significantly influenced by the anion content of the corresponding salt. Specifically, the content of cations should not exceed 25% of the total cation content, with the exception of silica–alumina. The addition of excess strontium salts does not enhance the Sr solidification process, but rather decreases the relative concentration of the alkali activator, resulting in incomplete dissolution of silica–alumina tetrahedra, which are necessary for

zeolite formation. Additionally, Sr curing can also occur via the formation of a new strontium feldspar phase ( $\text{SrAl}_2\text{Si}_2\text{O}_8$ ). However, its curing effect is not as satisfactory as that of cancrinite, and further research is necessary to investigate its content and structural stability. To ensure adequate curing of  $\text{Sr}^{2+}$  within the crystal structure of cancrinite, the optimal Sr/Al(Si) ratio should be maintained below 1/6.

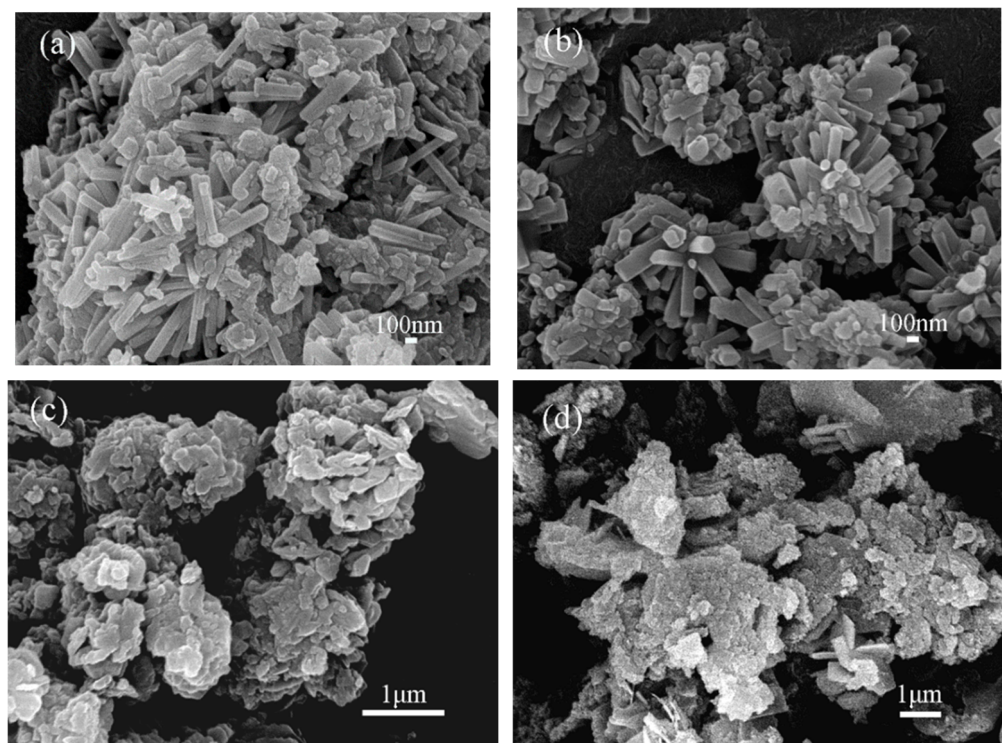


**Figure 10.** SEM photos of specimens obtained under different Sr/Al(Si) ratios when NaOH concentration, crystallization temperature, and crystallization time were 6 M, 180 °C, and 24 h, respectively (Sr/Al(Si) ratios: (a) 1/6, (b) 1/3, (c) 1/2, and (d) 2/3).

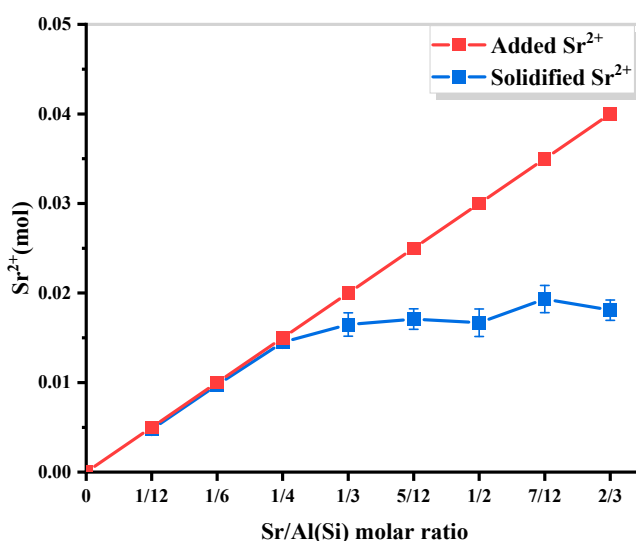


**Figure 11.** Content of added and solidified  $\text{Sr}^{2+}$ .

### 3.4. $\text{Sr}^{2+}$ Solidification and Leaching Test

Based on the above experimental results, Sr-cancrinite [ $\text{Sr}_x\text{Na}_{8-2x}(\text{AlSiO}_4)_6(\text{NO}_3)_2$ ], where  $x$  ranges from 0.2 to 1, was successfully synthesized through hydrothermal treatment

of CG as the main raw material at 180 °C for 24 h. The immobilization effectiveness of radioactive elements primarily depends on the structure of the main mineral phase of the immobilized material. X-ray diffraction analysis (Figure 12) confirmed that the synthesized sample exhibited a pure and stable cancrinite phase when  $x < 1$ .

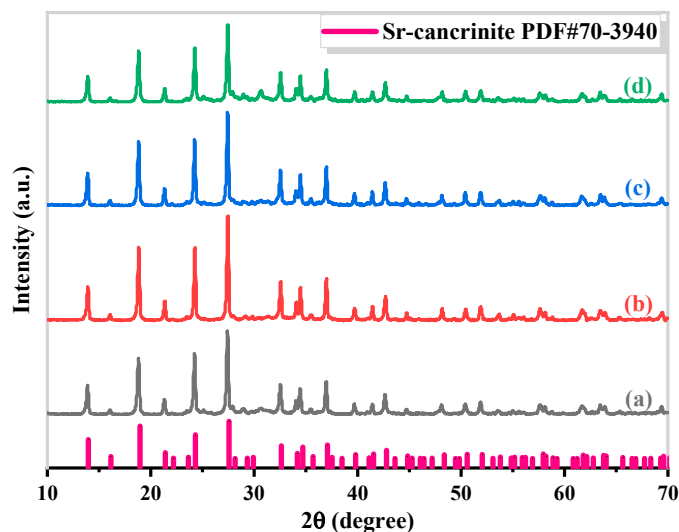


**Figure 12.** XRD patterns of solidified cancrinite waste specimens ( $x$  of  $\text{Sr}_x\text{Na}_{8-2x}(\text{AlSiO}_4)_6(\text{NO}_3)_2$ : (a) 0.2, (b) 0.4, (c) 0.6, (d) 0.8, and (e) 1).

This finding suggests that Sr-cancrinite can effectively stabilize waste materials under complex natural conditions while preventing the migration of nuclide ions into the environment.

The ion leaching concentrations of Sr-cancrinite, obtained using the PCT method, are presented in Table 2.

**Table 2.** Ion leaching concentrations of cancrinite according to PCT.

Sample	Mass Ratio of $\text{Sr}^{2+}$ (wt%)	Normalized Concentration (mg/L)	Solidification Rate (%)
$\text{Na}_8[(\text{SiAl})_6\text{O}_{12}](\text{NO}_3)_2$	0	0.000	-
$\text{Sr}_{0.2}\text{Na}_{7.6}[(\text{SiAl})_6\text{O}_{12}](\text{NO}_3)_2$	1.63	2.217	>99.9
$\text{Sr}_{0.4}\text{Na}_{7.2}[(\text{SiAl})_6\text{O}_{12}](\text{NO}_3)_2$	3.24	3.795	>99.9
$\text{Sr}_{0.6}\text{Na}_{6.8}[(\text{SiAl})_6\text{O}_{12}](\text{NO}_3)_2$	4.82	4.561	>99.9
$\text{Sr}_{0.8}\text{Na}_{6.4}[(\text{SiAl})_6\text{O}_{12}](\text{NO}_3)_2$	6.38	5.484	>99.9
$\text{SrNa}_6[(\text{SiAl})_6\text{O}_{12}](\text{NO}_3)_2$	7.92	6.190	>99.9

The normalized elemental mass release of  $\text{Sr}^{2+}$  from the samples was consistently low, typically less than that of boroaluminate glasses and calcined ceramics evaluated in other environmental assessments [11]. The solidification effectiveness did not diminish with the increasing  $\text{Sr}^{2+}$  content. When the  $\text{Sr}^{2+}$  content was increased to 7.92%, the normalized concentration of leached  $\text{Sr}^{2+}$  from the cancrinite specimens remained extremely low (6.190 mg/L), and the solidification rate (ratio of solidified Sr content to the total amount) of  $\text{Sr}^{2+}$  was nearly 100%. These results indicate that cancrinite waste forms possess excellent chemical durability, making them a promising candidate for the immobilization of radioactive elements.

#### 4. Conclusions

This paper reports on the successful synthesis of cancrinite crystals capable of immobilizing  $\text{Sr}^{2+}$  through hydrothermal treatment in an alkaline medium, using CG as the raw material. The study employed XRD, SEM, and PCT leaching tests to evaluate the effectiveness of the synthesized cancrinite crystals in immobilizing  $\text{Sr}^{2+}$ . The findings suggest that

stable and efficient immobilization of  $\text{Sr}^{2+}$  in the crystal structure of the cancrinite can be achieved by controlling the  $\text{NaOH}$  concentration at 6 M, the hydrothermal temperature at 180 °C, the hydrothermal time at 24 h, and the molar ratio of  $\text{Sr}/\text{Al}(\text{Si})$  at less than 1/6. The resulting cancrinite crystals exhibit low leaching of Sr and demonstrate good thermal and chemical stability.

Compared to traditional curing methods, the hydrothermal treatment method offers several advantages, including simplicity, rapidity, and good feasibility for emergency curing processes in nuclear accidents. The raw material employed is coal gangue, a readily available and cost-effective form of common waste. Furthermore, in comparison to glass and ceramic solidifications, this method exhibits a lower sintering temperature, which is below the boiling point of Sr (approximately 1000 °C) [42]. Consequently, issues such as flux selection and low-temperature densification sintering are alleviated. These findings provide new insights into the potential applications of cancrinite crystals for immobilizing  $\text{Sr}^{2+}$  and offer a promising approach to mitigate the risks associated with nuclear waste management.

To ensure the viability of this method, the radiation durability of the samples will be tested in subsequent studies. The plan involves simulating the  $\beta$  rays released during the decay of  $^{90}\text{Sr}$  and using our accelerator equipment to investigate the sample's resistance to irradiation. This approach aims to provide a more comprehensive understanding of the sample's performance under radiation exposure.

**Author Contributions:** Conceptualization, H.W., F.Z. and D.R.; methodology, H.W. and F.Z.; software, H.W. and F.Z.; validation, H.W., F.Z., R.A. and D.R.; formal analysis, H.W. and F.Z.; investigation, H.W. and F.Z.; resources, R.A. and D.R.; data curation, F.Z., R.A. and D.R.; writing—original draft preparation, H.W., F.Z. and D.R.; writing—review and editing, H.W., F.Z. and R.A.; visualization, H.W. and F.Z.; supervision, D.R.; project administration, D.R.; funding acquisition, D.R. All authors have read and agreed to the published version of the manuscript.

**Funding:** This work was supported by the National Natural Science Foundation of China (grant number: 11605116).

**Institutional Review Board Statement:** Not applicable.

**Informed Consent Statement:** Not applicable.

**Data Availability Statement:** The data are contained within the article.

**Conflicts of Interest:** The authors declare no conflicts of interest.

## References

1. International Atomic Energy Agency. *Country Nuclear Power Profiles*; International Atomic Energy Agency: Vienna, Austria, 2022.
2. Deutch, J.M.; Forsberg, C.W.; Kadak, A.C.; Kazimi, M.S.; Moniz, E.J.; Parsons, J.E.; Du, Y.; Pierpoint, L. *Update of the MIT 2003 Future of Nuclear Power*; Report for Massachusetts Institute of Technology; Massachusetts Institute of Technology: Cambridge, MA, USA, 2009.
3. Hamidouche, T.; Bousbia-Salah, A.; Si-Ahmed, E.K.; D'Auria, F. Overview of accident analysis in nuclear research reactors. *Prog. Nucl. Energy* **2008**, *50*, 7–14. [[CrossRef](#)]
4. Inan, S. Inorganic ion exchangers for strontium removal from radioactive waste: A review. *J. Radioanal. Nucl. Chem.* **2022**, *331*, 1137–1154. [[CrossRef](#)]
5. Ojovan, M.I. Nuclear Waste Disposal. *Encyclopedia* **2023**, *3*, 419–429. [[CrossRef](#)]
6. Hirose, K.; Igarashi, Y.; Aoyama, M. Analysis of the 50-year records of the atmospheric deposition of long-lived radionuclides in Japan. *Appl. Radiat. Isot. Incl. Data Instrum. Methods Use Agric. Ind. Med.* **2008**, *66*, 1675–1678. [[CrossRef](#)] [[PubMed](#)]
7. Shao, Y.; Yang, G.S.; Tazoe, H.; Ma, L.L.; Yamada, M.; Xu, D.D. A review of measurement methodologies and their applications to environmental  $^{90}\text{Sr}$ . *J. Environ. Radioact.* **2018**, *192*, 321–333. [[CrossRef](#)] [[PubMed](#)]
8. Pollock, D.W. Simulation of fluid-flow and energy-transport processes associated with high-level radioactive-waste disposal in unsaturated alluvium. *Water Resour. Res.* **1986**, *22*, 765–775. [[CrossRef](#)]
9. Oettingen, M. The Application of Radiochemical Measurements of PWR Spent Fuel for the Validation of Burnup Codes. *Energies* **2022**, *15*, 3041. [[CrossRef](#)]
10. Caurant, D.; Loiseau, P.; Majerus, O.; Aubin-Chevaldonnet, V.; Quintas, A. *Glasses, Glass-Ceramics and Ceramics for Immobilization of Highly Radioactive Nuclear Wastes*; Nova Science: Hauppauge, NY, USA, 2009.
11. Donald, I.W.; Metcalfe, B.L.; Taylor, R.N.J. The immobilization of high level radioactive wastes using ceramics and glasses. *J. Mater. Sci.* **1997**, *32*, 5851–5887. [[CrossRef](#)]

12. Jostsons, A.; Reeve, K.D. Immobilization of high level waste in Synroc. *Trans. Am. Nucl. Soc.* **1988**, *56* (Suppl. 1), 537–544.
13. Kyong Won, H.; Heinonen, J.; Bonne, A. Radioactive waste disposal: Global experience and challenges. *IAEA Bull.* **1997**, *39*, 33–41.
14. Ojovan, M.I.; Lee, W.E.; Kalmykov, S.N. Chapter 20—Ceramics and Novel Technologies. In *An Introduction to Nuclear Waste Immobilisation*, 3rd ed.; Ojovan, M.I., Lee, W.E., Kalmykov, S.N., Eds.; Elsevier: Amsterdam, The Netherlands, 2019; pp. 369–395.
15. Ringwood, A.E.; Kesson, S.E.; Ware, N.G.; Hibberson, W.; Major, A. Immobilization of high-level nuclear-reactor wastes in synroc. *Nature* **1979**, *278*, 219–223. [[CrossRef](#)]
16. Lutze, W.; Ewing, R.C. *Radioactive Waste Forms for the Future*; North-Holland: Amsterdam, The Netherlands, 1988.
17. Poitrasson, F.; Hanchar, J.M.; Schaltegger, U. The current state and future of accessory mineral research. *Chem. Geol.* **2002**, *191*, 3–24. [[CrossRef](#)]
18. Vance, E. Development of ceramic waste forms for high-level nuclear waste over the last 30 years. In Proceedings of the 30th Symposium on Scientific Basis for Nuclear Waste Management, Boston, MA, USA, 27 November–1 December 2006; Materials Research Society: Warrendale, PA, USA, 2007; Volume 985, pp. 137–144.
19. Weber, W.J.; Navrotsky, A.; Stefanovsky, S.; Vance, E.R.; Vernaz, E. Materials Science of High-Level Nuclear Waste Immobilization. *MRS Bull.* **2009**, *34*, 46–53. [[CrossRef](#)]
20. Šenilă, M.; Neag, E.; Tănăselia, C.; Šenilă, L. Removal of Cesium and Strontium Ions from Aqueous Solutions by Thermally Treated Natural Zeolite. *Materials* **2023**, *16*, 2965. [[CrossRef](#)]
21. Bonaccorsi, E.; Merlini, S. Modular microporous minerals: Cancrinite-Davyne group and C-S-H phases. In *Micro- and Mesoporous Mineral Phases*; Ferraris, G., Merlini, S., Eds.; Reviews in Mineralogy & Geochemistry; Mineralogical Society of America & Geochemical Society: Chantilly, VA, USA, 2005; Volume 57, pp. 241–290.
22. Gatta, G.D.; Lotti, P. Cancrinite-group minerals: Crystal-chemical description and properties under non ambient conditions—A review. *Am. Miner.* **2016**, *101*, 253–265. [[CrossRef](#)]
23. Hassan, I.; Antao, S.M.; Parise, J.B. Cancrinite: Crystal structure, phase transitions, and dehydration behavior with temperature. *Am. Miner.* **2006**, *91*, 1117–1124. [[CrossRef](#)]
24. Ballirano, P.; Maras, A.; Buseck, P.R. Crystal chemistry and IR spectroscopy of Cl- and SO<sub>4</sub>-bearing cancrinite-like minerals. *Am. Miner.* **1996**, *81*, 1003–1012. [[CrossRef](#)]
25. Chukanov, N.V.; Nedelko, V.V.; Blinova, L.N.; Korshunova, L.A.; Olysynch, L.V.; Lykova, I.S.; Pekov, I.V.; Buhl, J.C.; Depmeier, W. The role of additional anions in microporous aluminosilicates with cancrinite-type framework. *Russ. J. Phys. Chem. B* **2012**, *6*, 593–600. [[CrossRef](#)]
26. Chorover, J.; Choi, S.; Rotenberg, P.; Serne, R.J.; Rivera, N.; Strepka, C.; Thompson, A.; Mueller, K.T.; O'Day, P.A. Silicon control of strontium and cesium partitioning in hydroxide-weathered sediments. *Geochim. Cosmochim. Acta* **2008**, *72*, 2024–2047. [[CrossRef](#)]
27. Deng, Y.J.; Flury, M.; Harsh, J.B.; Felmy, A.R.; Qafoku, O. Cancrinite and sodalite formation in the presence of cesium, potassium, magnesium, calcium and strontium in Hanford tank waste simulants. *Appl. Geochem.* **2006**, *21*, 2049–2063. [[CrossRef](#)]
28. Deng, Y.J.; Harsh, J.B.; Flury, M.; Young, J.S.; Boyle, J.S. Mineral formation during simulated leaks of Hanford waste tanks. *Appl. Geochem.* **2006**, *21*, 1392–1409. [[CrossRef](#)]
29. Mon, J.; Deng, Y.J.; Flury, M.; Harsh, J.B. Cesium incorporation and diffusion in cancrinite, sodalite, zeolite, and allophane. *Microporous Mesoporous Mat.* **2005**, *86*, 277–286. [[CrossRef](#)]
30. Armstrong, J.A.; Dann, S.E. Investigation of zeolite scales formed in the Bayer process. *Microporous Mesoporous Mat.* **2000**, *41*, 89–97. [[CrossRef](#)]
31. Hermeler, G.; Buhl, J.C.; Hoffmann, W. The influence of carbonate on the synthesis of an intermediate phase between sodalite and cancrinite. In Proceedings of the 2nd German Workshop on Zeolite Chemistry, Hamburg, Germany, 21–22 March 1990; Elsevier Science Publisher B.V.: Amsterdam, The Netherlands, 1991; pp. 415–426.
32. Passos, F.; Castro, D.C.; Ferreira, K.K.; Simoes, K.M.A.; Bertolino, L.C.; Barbato, C.N.; Garrido, F.M.S.; Felix, A.A.S.; Silva, F. Synthesis and Characterization of Sodalite and Cancrinite from Kaolin. In Proceedings of the TMS Annual Meeting and Exhibition/Symposium on Characterization of Minerals, Metals, and Materials, San Diego, CA, USA, 7 February 2017; Springer International Publishing: Cham, Switzerland, 2017; pp. 279–288. [[CrossRef](#)]
33. Xu, B.A.; Giles, D.E.; Ritchie, I.M. Reactions of lime with carbonate-containing solutions. *Hydrometallurgy* **1998**, *48*, 205–224. [[CrossRef](#)]
34. Baic, I.; Witkowska-Kita, B. Hard Coal Mining Waste Management Technologies—Diagnosis of Current Development, Innovativeness Evaluation and SWOT Analysis. *Roczn. Ochr. Środowiska* **2011**, *13*, 1315–1325.
35. Bian, Z.; Inyang, H.I.; Daniels, J.L.; Otto, F.; Struthers, S. Environmental issues from coal mining and their solutions. *Min. Sci. Technol.* **2010**, *20*, 215–223. [[CrossRef](#)]
36. Yu, L.J.; Feng, Y.L.; Yan, W. The current situation of comprehensive utilization of coal gangue in China. In Proceedings of the 1st International Conference on Energy and Environmental Protection (ICEEP 2012), Hohhot, China, 23–24 June 2012; Trans Tech Publications Ltd.: Stafa-Zurich, Switzerland, 2012; Volume 524–527, pp. 915–918. [[CrossRef](#)]
37. Li, J.Y.; Wang, J.M. Comprehensive utilization and environmental risks of coal gangue: A review. *J. Clean. Prod.* **2019**, *239*, 18. [[CrossRef](#)]

38. Pekov, I.V.; Olysynch, L.V.; Chukanov, N.V.; Zubkova, N.V.; Pushcharovsky, D.Y.; Van, K.V.; Giester, G.; Tillmanns, E. Crystal chemistry of cancrinite-group minerals with an AB-type framework: A review and new data. I. chemical and structural variations. *Can. Mineral.* **2011**, *49*, 1129–1150. [[CrossRef](#)]
39. ASTM International C 1285-14; Standard Test Methods for Determining Chemical Durability of Nuclear, Hazardous, and Mixed Waste Glasses and Multiphase Glass Ceramics: The Product Consistency Test (PCT). ASTM International: West Conshohocken, PA, USA, 1997.
40. Kim, J.K.; Lee, H.D. Effects of step change of heating source on synthesis of zeolite 4A from coal fly ash. *J. Ind. Eng. Chem.* **2009**, *15*, 736–742. [[CrossRef](#)]
41. Maenami, H.; Shin, H.; Ishida, H.; Mitsuda, T. Hydrothermal solidification of wastes with formation of zeolites. *J. Mater. Civ. Eng.* **2000**, *12*, 302–306. [[CrossRef](#)]
42. Lee, W.E.; Ojovan, M.I.; Stennett, M.C.; Hyatt, N.C. Immobilisation of radioactive waste in glasses, glass composite materials and ceramics. *Adv. Appl. Ceram.* **2006**, *105*, 3–12. [[CrossRef](#)]

**Disclaimer/Publisher's Note:** The statements, opinions and data contained in all publications are solely those of the individual author(s) and contributor(s) and not of MDPI and/or the editor(s). MDPI and/or the editor(s) disclaim responsibility for any injury to people or property resulting from any ideas, methods, instructions or products referred to in the content.